Available online at www.sciencedirect.com
ScienceDirect
Computers and Mathematics with Applications 54 (2007) 242–254
An International Journal
computers & mathematics
with applications
www.elsevier.com/locate/camwa

A study of solitary waves in a tapered aorta by using the theory of solitons

J.C. Misra*, M.K. Patra

Center for Theoretical Studies, Indian Institute of Technology, Kharagpur-721302, India

Received 26 October 2006; accepted 12 December 2006

Abstract

By applying the soliton theory, a method is developed in this paper with an aim to study the flow properties of blood in large blood vessels. The theory takes into account the nonlinear terms of the Navier–Stokes equations as well as the large deformations of the aortic wall. The solutions of the equations of motion are restricted to the propagation of axisymmetric long waves. As for the equations governing the motion of the aorta, the longitudinal motion of the aortic wall is considered negligible. The radial motion is obtained directly from the pressure wave and the material behaviour of the aorta, by considering the motion of an elementary volume of the wall tissues. By using the experimentally measured values of the system parameters, computational work has been carried out to examine the change in radius, rate of change of radius, the dependence of the radius of the aorta on the longitudinal distance and the axial velocity distribution of blood in the aorta within a cardiac cycle. Variation of the stroke volume of the blood pulse is also determined for different taper angles of the aorta.

Keywords: Solitary waves; Solitons; Aorta; Stroke volume; Dispersion relation

1. Introduction

One of the most striking features of the arterial blood flow is its pulsatile character. The intermittent ejection of blood from the left ventricle of the heart produces pressure and flow pulses in the arterial tree. Experimental studies of these pulses reveal that the velocity of blood is largely dependent on the elastic properties of the arterial wall [1]; some modification takes place as the pulses propagate towards the periphery in a characteristic pattern [2].

As is the case with most problems of life sciences, the phenomenon of blood flow in arteries is quite complex. Analytical treatment of the associated problems has been subjected to constant changes; modifications have been made through improved experimental measurements. According to Jones et al. [3], wave fronts in arterial blood flow may travel forward towards the periphery or backward, that is, towards the heart after reflection. Changes in pressure $p(z, t)$ and uniform velocity $v(z, t)$ due to forward wave fronts are in the same sense (cf. Fig. 1), so that a forward wave front with positive pressure change, termed as a compression wave front, accelerates the flow whereas a forward wave front with negative pressure change, called an expansion wave front, decelerates the flow. Conversely, backward wave fronts induce opposite changes in pressure and velocity.

* Corresponding author. Fax: +91 3222 55303.
E-mail address: jcm@maths.iitkgp.ernet.in (J.C. Misra).

0898-1221/$ - see front matter © 2007 Elsevier Ltd. All rights reserved.
doi:10.1016/j.camwa.2006.12.025

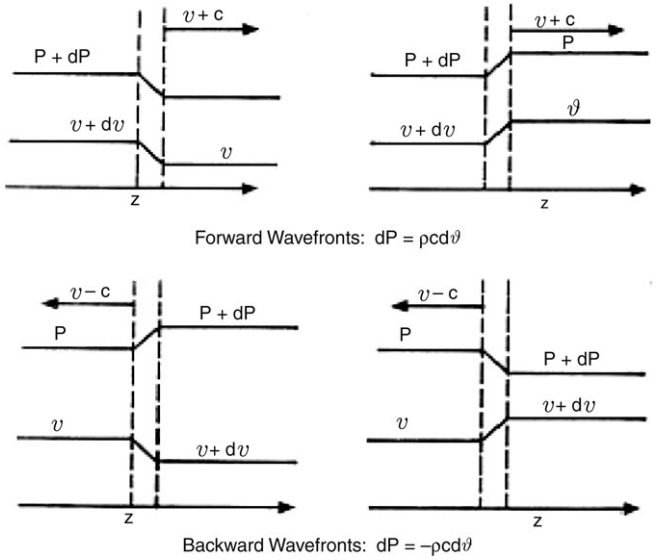

Fig. 1. Pressure and velocity changes associated with forward and backward compression and expansion wave fronts.

Viscous as well as inertial properties of blood were first taken into account in some elastic tube model studies. Cox [4] studied the effect of initial stresses and perivascular tethering as well as the orthotropic viscoelastic behaviour of the arterial wall on the flow of blood. Noubissie and Woafo [5] studied the dynamical behaviour of waves in thin tapered elastic tubes with localized deformations. They made an observation that the amplitude of velocity waves decreases along the tube as the tube radius decreases. The propagation of waves in a fluid-filled prestressed thin elastic tube subjected to a uniform internal pressure was investigated by Demiray and Dost [6]. They also considered a physiological application of their analysis. A similar study was made by Demiray [7] who analysed theoretically the propagation of solitary waves in a prestressed thin elastic tube. On the basis of his analysis he tried to make some observations on the flow of blood through arteries, by considering axial tethering but neglecting the effect of axial displacement. Hashizume [8] and Yomosa [9] studied propagation of solitary waves in arteries by using nonlinear elasticity theory, by neglecting the evolution of the elastic properties of arterial walls.

Womersley's theory and its extensions are based on the linearized Navier–Stokes equations and small basic deformations. Although earlier studies with linearized Navier–Stokes equations and small basic deformations have been found to be somewhat satisfactory in describing certain aspects of the flow in small arteries [10], they fail to give an adequate representation of the flow field in large arteries (cf. [11–15]), the walls of which undergo large deformation owing to the large dynamic storage effect. As a result of this, both the geometric and elastic nonlinear effects come into play [16].

In order to account for the aforesaid factors, an approximate method has been developed here for the study of solitary wave motion of blood in an aortic vessel. Analytical estimates are obtained for the change of radius, rate of change of radius, change of radius of the aorta with longitudinal distance and the axial velocity distribution of blood in the aortic segment within a cardiac period. The variation of the stroke volume of the blood pulse is also examined for various taper angles of the aorta.

2. Flow equations

In order to determine a flow field one has to solve a system of simultaneous equations which govern both the motion of the blood and the motion of the arterial wall. The analysis of such a system is very much involved. Previous experimental studies [1,17] indicate that for blood flow problem the effect of the convective acceleration terms in the Navier–Stokes equation dominates over that of the viscous forces. The convective accelerations are partly generated locally by the vessel taper (both the natural taper and the generated taper due to the propagation of wave fronts) as well as the radial motion of the vessel wall and partly due to the connection of momentum defect from upstream. This

latter part, commonly called the entrance effect, is most pronounced near branches and bifurcations. Unlike the case of rigid cylindrical tubes, the entrance effect in distensible blood vessels is confined to a length less than ten diameters distal from branches [12]. Therefore flows which are not close to major branches, such as those in the descending thoracic aorta, can be considered as fully developed.

In this study of large amplitude wave propagation in blood vessels, we postulate one-dimensional motion of blood and consider the pressure as well as the flow velocity to be uniform over the entire region of each normal cross-section. This is an approximation of the real situation and it implies that we are essentially considering the spatial average values of the dependent flow variables at each cross-section. We also model the aorta as a straight tapered elastic tube and blood as an incompressible Newtonian fluid; the effects of viscosity are accounted for in an appropriate manner. The cross-section of the aorta is taken to be circular and the flow to be axially symmetric at the chosen site.

We take cylindrical coordinates (r, θ, z), where the z-axis is taken along the axis of the aorta, the radial direction being perpendicular to it and the origin being taken at the midpoint of the fully developed flow region. For conservation of momentum, we write

$$\frac{\partial v}{\partial t} + v\frac{\partial v}{\partial z} + \frac{1}{\rho}\frac{\partial p}{\partial z} = \nu\frac{\partial^2 v}{\partial z^2} \tag{1}$$

where ρ is the density and ν the kinematic viscosity of blood. From the measurements of flow pulses in canine arteries, it is known that the pulse wave velocity $V' \approx 550$ cm/s, the maximum velocity of blood $v^* \approx 110$ cm/s and the time required for the flow velocity to increase from 0 to v^* is $T' \approx 0.05$ s. The ratio between the viscous term and the nonlinear term is $\frac{\mu}{\rho}\frac{\partial^2 v}{\partial z^2}/v\frac{\partial v}{\partial z} \approx \frac{\mu}{\rho V' T' v^*} \approx o(10^{-5})$, where $\mu = 0.04p$ and $\rho = 1.05$ g/cm^3. Thus the viscous effect turns out to be negligible in comparison to the nonlinear effect.

Conservation of mass of blood requires that the rate of increase of mass inside a blood vessel segment of unit length is equal to the net influx of mass. For an incompressible fluid, we have

$$\frac{\partial A}{\partial t} + \frac{\partial}{\partial z}(Av) + \Psi = 0 \tag{2}$$

where $A = A(z, t)$ stands for the cross-sectional area of the blood vessel, Ψ is the rate of volumetric outflow (leakage) per unit length of the vessel through discrete bifurcations and branches. In the context of our present study, we may assume $\Psi = 0$.

3. Wall motion

Experimental studies reveal that the longitudinal motion of blood vessels is very small [18]. This is attributed mainly to strong vascular tethering [19,20] and partly to the predominantly circumferential orientation of the elastin and collagen fibers [21] which minimizes the coupling between circumferential and longitudinal strains. The experimental study by Patel et al. [18] shows further that the inertial force due to the effective mass of the aortic vessel wall is negligible compared to both the pressure and the elastic forces.

The radial motion of the aortic wall can thus be obtained directly from the pressure wave and the material behaviour of the vessel. The equation governing the motion of the wall can be derived as stated below.

We consider a small segment of the vessel wall surrounded by inner and outer surfaces of the wall and two parallel cross-sectional surfaces perpendicular to the z-axis defined by constant axial coordinates z and $z + \mathrm{d}z$ and two surfaces defined by constant circumferential angles θ and $\theta + \mathrm{d}\theta$ (cf. Fig. 2(a)). The equation that governs the radial motion of this small segment can be written as

$$\rho_0(R\mathrm{d}\theta h'\mathrm{d}z)\frac{\partial^2 R}{\partial t^2} = (P - P_A)\cos\alpha(R\mathrm{d}\theta\mathrm{d}l) - 2\sigma_t \sin(\mathrm{d}\theta/2)h\mathrm{d}z + \frac{\partial}{\partial z}(\sigma_1 \sin\alpha)\mathrm{d}z(hR\mathrm{d}\theta) \tag{3}$$

where ρ_0 denotes the material density of the wall, $R = R(z, t)$ the radius of the tube, h' the actual thickness and h the thickness of the wall in radial direction in which the material undergoes elastic deformation; h and h' are connected through the relation $h' = h\cos\alpha$, P_A the atmospheric pressure, σ_t the extending stress in the direction of the meridian line on the wall surface, α the natural semi-angle of taper of the vessel and $\mathrm{d}l$ the elementary length of the meridian line (cf. Figs. 2(b) and 2(c)).

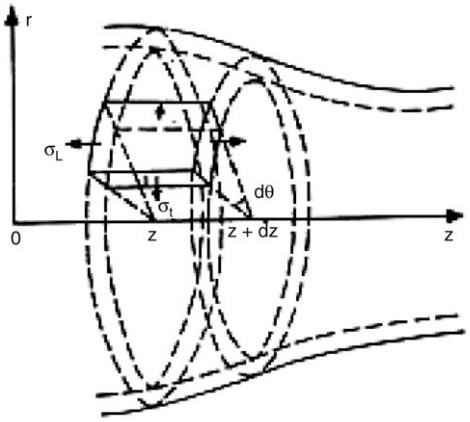

Fig. 2(a). A small segment of the aortic wall.

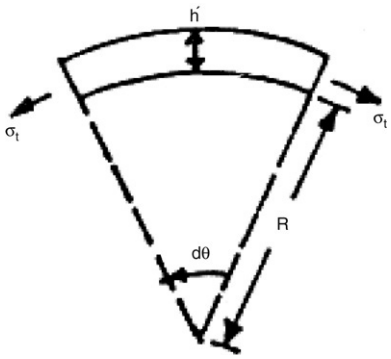

Fig. 2(b). Extending stress in the longitudinal direction on the wall surface.

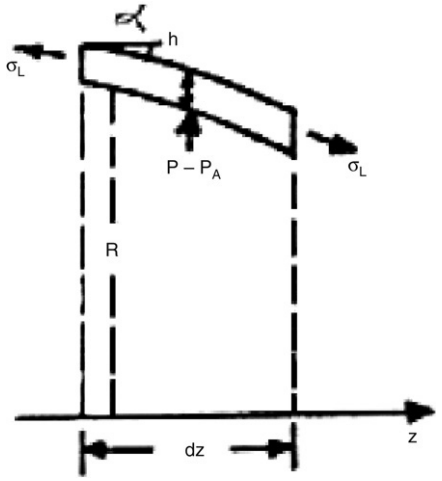

Fig. 2(c). Longitudinal extending stress in the direction of the meridian line on the wall surface.

Since α is very small, we may assume $\cos\alpha \approx 1$ and $\alpha \approx \sin\alpha \approx \tan\alpha = -\frac{\partial R}{\partial z}$. Then $\frac{\partial}{\partial z}(\sigma_1 \sin\alpha) \approx -E_1 \frac{\partial}{\partial z}(\frac{\mathrm{d}l-\mathrm{d}z}{\mathrm{d}z}\frac{\partial R}{\partial z}) \approx -\frac{3E_1}{2}(\frac{\partial R}{\partial z})^2 \frac{\partial^2 R}{\partial z^2}$, where E_1 is the Young's modulus in longitudinal elastic deformation of the

wall. For small angle $d\theta$, we approximate $\sin(d\theta/2) \approx d\theta/2$, as a consequence of which Eq. (3) reduces to

$$\rho_0 h \frac{\partial^2 R}{\partial t^2} = (P - P_A) - \frac{h}{R}\sigma_t - \frac{3hE_1}{2}\left(\frac{\partial R}{\partial z}\right)^2 \frac{\partial^2 R}{\partial z^2}. \tag{4}$$

We write the radial displacement u of the aortic wall as

$$R = R_0 - z\tan\alpha + u. \tag{5}$$

Then the elastic property of the wall (including the nonlinear elastic effects) may be represented by

$$\sigma_t = E\frac{u}{R_0 - z\tan\alpha}\left(1 + \frac{au}{R_0 - z\ \tan\alpha}\right) \tag{6}$$

where E and a are respectively the Young's modulus and the nonlinear coefficient of elasticity. R_0 denotes the equilibrium radius of the aortic segment at the origin. It may be mentioned that since as per experimental observations, the longitudinal motion of the aortic wall is quite small in comparison to the radial motion, Hooke's Law is adequate for the longitudinal direction, whereas for the circumferential direction a quadratic law has been used. Owing to the conservation of mass of the tissue, we have

$$Rh = R_0 h_0 \tag{7}$$

where h_0 stands for the equilibrium value of h. Using (6) and (7), we have from (4) the equation

$$\rho_0 h_0 \frac{\partial^2 u}{\partial t^2} + \frac{h_0 E u(R_0 - z\tan\alpha + au)}{(R_0 - z\tan\alpha + u)(R_0 - z\tan\alpha)^2} - (P - P_A)\left(1 + \frac{u - z\tan\alpha}{R_0}\right) + \frac{3h_0E_1}{2}\left(\frac{\partial u}{\partial z} - \tan\alpha\right)^2 \frac{\partial^2 u}{\partial z^2} = 0. \tag{8}$$

4. The solution

In view of the relation (5), the Eq. (2) may be rewritten as

$$\frac{\partial u}{\partial t} + \frac{R_0}{2}\left(1 + \frac{u - z\tan\alpha}{R_0}\right)\frac{\partial v}{\partial z} + v\left(\frac{\partial v}{\partial z} - \tan\alpha\right) = 0. \tag{9}$$

We now introduce dimensionless variables z', t', $\bar{v}$, $\bar{p}$ and $\bar{u}$ defined through the relations

$$z = L_0 z', \qquad t = T_0 t', \qquad v = C_0\bar{v}, \qquad p - p_A = p_0\bar{p}, \qquad u = R_0\bar{u} \tag{10}$$

in which

$$L_0 = (h_0\rho_0 R_0/2\rho)^{1/2}, \qquad T_0 = (\rho_0 R_0^2/E)^{1/2}, \qquad p_0 = Eh_0/R_0 \quad \text{and} \quad C_0 = 2L_0/T_0. \tag{11}$$

The three fundamental equations (1), (9) and (8) in their non-dimensional form read

$$\frac{\partial\bar{v}}{\partial t'} + 2\bar{v}\frac{\partial\bar{v}}{\partial z'} + \frac{\partial\bar{p}}{\partial z'} = 0 \tag{12}$$

$$\frac{\partial\bar{u}}{\partial t'} + 2\bar{v}\left(\frac{\partial\bar{u}}{\partial z'} - \frac{L_0\alpha}{R_0}\right) + \left(1 + \bar{u} - \frac{L_0 z'\alpha}{R_0}\right)\frac{\partial\bar{v}}{\partial z'} = 0 \tag{13}$$

$$\frac{\partial^2\bar{u}}{\partial t'^2} - \bar{p}\left(1 + \bar{u} - \frac{L_0 z'\alpha}{R_0}\right) + \frac{\bar{u}(1 + a\bar{u} - L_0 z'\alpha/R_0)}{1 + \bar{u} - L_0 z'\alpha(3 + 2\bar{u})/R_0} - K_0\left(\frac{\partial\bar{u}}{\partial z'} - \frac{L_0\alpha}{R_0}\right)^2\frac{\partial^2\bar{u}}{\partial z'^2} = 0 \tag{14}$$

with $K_0 = (6E_1R_0^2\rho^2)/(Eh_0^2\rho_0^2)$. At the end of a diastole, blood pressure attains its lowest value. Let us denote the aortic pressure and the radial displacement by p_0 and u_0 respectively. Then we obtain the relations

$$p_0 - p_A = p_0\bar{p}_0 \quad \text{and} \quad u_0 = R_0\bar{u}_0. \tag{15}$$

To study the asymptotic behaviour of nonlinear dispersive waves, Gardner and Morikawa [22] introduced the scale transformation with a perturbation expansion of the dependent variables. This type of perturbation was formulated for the long wave approximation in a general way and was called the reductive perturbation method (cf. [23–25]). Employing this method we write

$$\bar{p} = \bar{p_0} + \bar{\bar{p}}, \qquad \bar{u} = \bar{u}_0 + \bar{\bar{u}}. \tag{16}$$

Then the linearized forms of the Eqs. (12)–(14) are as follows:

$$\frac{\partial \bar{v}}{\partial t'} + \frac{\partial \bar{\bar{p}}}{\partial z'} = 0, \qquad \frac{\partial \bar{\bar{u}}}{\partial t'} + (1+\bar{u}_0)\frac{\partial \bar{v}}{\partial z'} = 0, \qquad \frac{\partial^2 \bar{\bar{u}}}{\partial t'^2} - (1+\bar{u}_0)\bar{\bar{p}} + g^2\bar{\bar{u}} = 0 \tag{17}$$

with

$$\bar{p_0} = \frac{\bar{u}_0(1+a\bar{u}_0)}{(1+\bar{u}_0)^2} \tag{18}$$

and

$$g^2 = \frac{1+(2a-1)\bar{u}_0}{(1+\bar{u}_0)^2}. \tag{19}$$

Some characteristic features of wave propagation in dispersive media can be seen even in linear approximation. The oscillations in question can be described by the set of quantities $\bar{v}, \bar{\bar{p}}, \bar{\bar{u}}$ which satisfy the set of linear partial differential equations derived from (12)–(14) with the use of (16). The general solution of the system of equations in linear approximation takes the form of a set of plane waves described by

$$(\bar{v}, \bar{\bar{p}}, \bar{\bar{u}}) = (A_1, A_2, A_3)\exp[\mathrm{i}\omega(t' - z'/c)] \tag{20}$$

where c is the local wave speed which is the velocity at which small disturbances are propagated relative to the fluid at rest, ω is the circular frequency and A_i $(i = 1, 2, 3)$ are the complex amplitudes of the system variables. The dispersion law $c = c(\omega)$ is determined by the system of basic equations. Substituting (20) in the aforesaid linearized equation (17), we get

$$cA_1 - A_2 = 0, \qquad (1+\bar{u}_0)A_1 - cA_3 = 0 \quad \text{and} \quad (1+\bar{u}_0)A_2 + (\omega^2 - g^2)A_3 = 0. \tag{21}$$

A nontrivial solution of (21) exists if and only if

$$\begin{vmatrix} c & -1 & 0 \\ 1+\bar{u}_0 & 0 & -c \\ 0 & 1+\bar{u}_0 & \omega^2 - g^2 \end{vmatrix} = 0$$

which gives the dispersion relation for this nonlinear problem as

$$c^2 = g^2 - \omega^2. \tag{22}$$

From (22), it follows that c is large when g is large and ω is small. To obtain an asymptotic estimate of the long waves, we expand $c(\omega)$ into a Taylor series about the origin for small values of ω/g. Neglecting terms of order $(\omega/g)^4$, we obtain $c^{-1} = g^{-1}(1 + \frac{w^2}{2g^2})$. Then $\exp[\mathrm{i}\omega(t' - z'/c)] = \exp[\mathrm{i}\{\frac{w}{g}(gt' - z') - (\frac{\omega}{g})^3\}]$. It has been demonstrated by Gardner and Morikawa [22] that the similarity of asymptotic behaviour holds for a coordinate transformation which satisfies the equation

$$(gt' - z')/z'^{\frac{1}{3}} = \text{constant}. \tag{23}$$

Let us introduce the scale transformation in terms of a small parameter ε for which (23) holds:

$$\xi = \varepsilon^{1/2}(gt' - z') \quad \text{and} \quad \eta = \varepsilon^{3/2}z'. \tag{24}$$

Then

$$\frac{\partial}{\partial z'} = \varepsilon^{1/2}\left(-\frac{\partial}{\partial \xi} + \varepsilon\frac{\partial}{\partial \eta}\right), \qquad \frac{\partial}{\partial t'} = \varepsilon^{1/2} g\frac{\partial}{\partial \xi},$$
$$\frac{\partial^2}{\partial z'^2} = \varepsilon\left(\frac{\partial^2}{\partial \xi^2} - 2\varepsilon\frac{\partial^2}{\partial \xi\,\partial \eta} + \varepsilon^2\frac{\partial^2}{\partial \eta^2}\right), \qquad \frac{\partial^2}{\partial t' 2} = \varepsilon g^2\frac{\partial^2}{\partial \xi^2}. \tag{25}$$

Choosing α to be so small that

$$L_0\alpha/R_0 = O(\varepsilon^{5/2}). \tag{26}$$

We introduce perturbation expansions of $\bar{v}$, $\bar{\bar{p}}$ and $\bar{\bar{u}}$ in terms of ε as follows:

$$\bar{v} = \varepsilon v_1(\xi,\eta) + \varepsilon^2 v_2(\xi,\eta) + \cdots$$
$$\bar{\bar{p}} = \varepsilon p_1(\xi,\eta) + \varepsilon^2 p_2(\xi,\eta) + \cdots$$
$$\bar{\bar{u}} = \varepsilon u_1(\xi,\eta) + \varepsilon^2 u_2(\xi,\eta) + \cdots. \tag{27}$$

Using the relations (16), (24) and (25), the nonlinear equations (12)–(14) may be written in terms of ξ and η as

$$g\frac{\partial \bar{v}}{\partial \xi} + 2\bar{v}\left(-\frac{\partial}{\partial \xi} + \varepsilon\frac{\partial}{\partial \eta}\right)\bar{v} + \left(-\frac{\partial}{\partial \xi} + \varepsilon\frac{\partial}{\partial \eta}\right)\bar{\bar{p}} = 0,$$
$$g\frac{\partial \bar{\bar{u}}}{\partial \xi} + 2\bar{v}\left[\left(-\frac{\partial}{\partial \xi} + \varepsilon\frac{\partial}{\partial \eta}\right)\bar{\bar{u}} - \varepsilon^2\right] + (1 + \bar{u}_0 + \bar{\bar{u}} - \varepsilon\eta)\left(-\frac{\partial}{\partial \xi} + \varepsilon\frac{\partial}{\partial \eta}\right)\bar{v} = 0,$$
$$\varepsilon^2 g^2\frac{\partial^2 \bar{\bar{u}}}{\partial \xi^2} - (\bar{p}_0 + \bar{\bar{p}})(1 + \bar{u_o} + \bar{\bar{u}} - \varepsilon\eta) + \frac{(\bar{u}_0 + \bar{\bar{u}})[1 + a(\bar{u}_0 + \bar{\bar{u}}) - \varepsilon\eta]}{1 + \bar{u}_0 + \bar{\bar{u}} - \varepsilon\eta[3 + 2(\bar{u}_0 + \bar{\bar{u}})]}$$
$$- K_0\varepsilon^2\left[\left(-\frac{\partial}{\partial \xi} + \varepsilon\frac{\partial}{\partial \eta}\right)\bar{\bar{u}} - \varepsilon^2\right]^2\left(\frac{\partial^2}{\partial \xi^2} - 2\varepsilon\frac{\partial^2}{\partial \xi\,\partial \eta} + \varepsilon^2\frac{\partial^2}{\partial \eta^2}\right)\bar{\bar{u}} = 0. \tag{28}$$

Substituting (27) into (28), the terms that are proportional to ε give rise to

$$g\frac{\partial v_1}{\partial \xi} - \frac{\partial p_1}{\partial \xi} = 0, \tag{29}$$
$$g\frac{\partial u_1}{\partial \xi} - (1 + \bar{u_o})\frac{\partial v_1}{\partial \xi} = 0 \tag{30}$$

and

$$\bar{p_0}(u_1 - \eta) + p_1(1 + \bar{u}_0) - \frac{(1 + 2a\bar{u}_0)u_1 - \bar{u}_0\eta}{1 + \bar{u}_0} + \frac{\bar{u}_0(1 + a\bar{u}_0)}{(1 + \bar{u}_0)^2}[u_1 - \eta(3 + 2\bar{u}_0)] = 0. \tag{31}$$

Integrating (29) and (30), we get

$$gv_1 = p_1 + c_1(\eta) \quad \text{and} \quad gu_1 = (1 + \bar{u}_0)v_1 + c_2(\eta) \tag{32}$$

where $c_1(\eta)$ and $c_2(\eta)$ are independent of ξ; they are to be determined from the boundary conditions. Our assumption that at the end of diastolic period, $p = p_0, \bar{u} = \bar{u}_0$ and $\bar{v} = 0$ allows us to conclude that $p_1 = 0$ and $u_1 = 0$ when $v_1 = 0$. Thus from (32), we have

$$v_1 = p_1/g = gu_1/(1 + \bar{u}_0). \tag{33}$$

Using (28), the terms that are proportional to ε^2 yield

$$g\frac{\partial v_2}{\partial \xi} - 2v_1\frac{\partial v_1}{\partial \xi} + \frac{\partial p_1}{\partial \eta} - \frac{\partial p_2}{\partial \xi} = 0, \tag{34}$$
$$g\frac{\partial u_2}{\partial \xi} - 2v_1\frac{\partial u_1}{\partial \xi} + (1 + \bar{u}_0)\left(\frac{\partial v_1}{\partial \eta} - \frac{\partial v_2}{\partial \xi}\right) - (u_1 + \eta)\frac{\partial v_1}{\partial \xi} = 0, \tag{35}$$

and

$$g^2\frac{\partial^2 u_1}{\partial \xi^2} - \bar{p}_0 u_2 - p_1(u_1+\eta) - p_2(1+\bar{u}_0) + \frac{(1+2a\bar{u}_0)u_2 + a u_1^2 + u_1\eta}{1+\bar{u}_0}$$
$$- \frac{(1+2a\bar{u}_0)u_1 + \bar{u}_0\eta}{(1+\bar{u}_0)^2}[u_1 + \eta(3+2\bar{u}_0)] + \frac{\bar{u}_0(1+a\bar{u}_0)}{1+\bar{u}_0}\left[\left\{\frac{u_1}{1+\bar{u}_0} + \frac{(\eta(3+2\bar{u}_0))}{1+\bar{u}_0}\right\}^2\right.$$
$$\left. - \frac{u_2}{1+\bar{u}_0} - \frac{2u_1\eta}{L+\bar{u}_0} - \frac{\eta^2(3+\bar{u}_0)}{1+\bar{u}_0}\right] = 0. \tag{36}$$

Eliminating v_2 between (34) and (35) and using (21) and (33), we obtain

$$\frac{g^2}{1+\bar{u}_0}\frac{\partial u_2}{\partial \xi} - 5v_1\frac{\partial v_1}{\partial \xi} + 2g\frac{\partial v_1}{\partial \eta} - \frac{g\eta}{1+\bar{u}_0}\frac{\partial v_1}{\partial \xi} - \frac{\partial p_2}{\partial \xi} = 0. \tag{37}$$

Further using the relations (21) and (33), we rewrite (36) as

$$g\frac{\partial^3 v_1}{\partial \xi^3} + \frac{g^2}{1+\bar{u}_0}\frac{\partial u_2}{\partial \xi} + \frac{2[(a-2)-(2a-1)\bar{u}_0]}{1+(2a-1)\bar{u}_0}v_1\frac{\partial v_1}{\partial \xi} - \frac{\partial p_2}{\partial \xi}$$
$$+ \frac{3+(8a-1)\bar{u}_0 + 6a\bar{u}_0^2 + 2a\bar{u}_0^3}{g(1+\bar{u}_0)^3}\eta\frac{\partial v_1}{\partial \xi} = 0. \tag{38}$$

In a similar manner, simultaneous elimination of p_2 and u_2 between (37) and (38) gives rise to the modified KdV equation

$$\frac{\partial v_1}{\partial \eta} - k v_1\frac{\partial v_1}{\partial \xi} - N\eta\frac{\partial v_1}{\partial \xi} - \frac{1}{2}\frac{\partial^3 v_1}{\partial \xi^3} = 0. \tag{39}$$

Similar KdV equations for p_1 and u_1 are obtained from Eqs. (29)–(32), viz.

$$\frac{\partial p_1}{\partial \eta} - L p_1\frac{\partial p_1}{\partial \xi} - N\eta\frac{\partial p_1}{\partial \xi} - \frac{1}{2}\frac{\partial^3 p_1}{\partial \xi^3} = 0 \tag{40}$$

and

$$\frac{\partial u_1}{\partial \eta} - M u_1\frac{\partial u_1}{\partial \xi} - N\eta\frac{\partial u_1}{\partial \xi} - \frac{1}{2}\frac{\partial^3 u_1}{\partial \xi^3} = 0 \tag{41}$$

where the constants K, L, M and N are defined by

$$K = \frac{(1+\bar{u}_0)[(2a+1)+3(2a-1)\bar{u}_0]}{2[1+(2a-1)\bar{u}_0]^{3/2}}, \quad K = gL = \frac{1+\bar{u}_0}{g}M$$
$$N = \frac{1+3a\bar{u}_0+3a\bar{u}_0^2+a\bar{u}_0^3}{(1+\bar{u}_0)[1+(2a-1)\bar{u}_0]}. \tag{42}$$

By using the transformations

$$v_1 = 3V/K, \qquad \xi = X, \qquad \eta = -2\zeta \quad \text{and} \quad N = \lambda/4. \tag{43}$$

Eq. (39) can be written in the standard form of the modified KdV equation

$$\frac{\partial V}{\partial \zeta} + 6V\frac{\partial V}{\partial X} - \lambda\zeta\frac{\partial V}{\partial X} + \frac{\partial^3 V}{\partial X^3} = 0. \tag{44}$$

The exact solution of this equation can be achieved by employing the inverse scattering method with an initial data (cf. [1,26–29]). The conditions: $p = p_0, v = 0$ for all z define an equilibrium state of our system, whereas

$p = p_0, v = 0$ at $z = \pm\infty$ may be regarded as boundary conditions for our dynamical problem. The unique soliton solution of the Eq. (44) is thus given by

$$V = 2K^2 \operatorname{sech}^2\left[k\left\{X - \left(4k^2\zeta^2 - \frac{\lambda}{2}\zeta^2\right)\right\} + \theta\right] \tag{45}$$

where k and θ are arbitrary constants. Solitary wave solution seems to explain the observed fact that 'steepening' in the arterial pulse wave occurs in accordance with the increase in pulse-wave velocity (cf. [30,31]). With the help of (11), (24), (27) and (43) the soliton solution (45) can be presented as

$$v(z,t) = \frac{6C_0\bar{k}^2}{k}\operatorname{sech}^2\left[\frac{g\bar{k}}{T_0}\left\{t - \frac{T_0}{gL_0}z(1-2\bar{k}^2) + \frac{\lambda\varepsilon^{\frac{5}{2}}z^2}{8gL_0^2}\right\} + \theta\right] \tag{46}$$

where $\bar{k} = \varepsilon^{1/2}k$. In a similar manner, using (15), (33) and (42), from Eqs. (40) and (41), the corresponding soliton solutions are obtained from the Eqs. (40) and (41), in the form

$$p(z,t) = p_0 + \frac{6p_0\bar{k}^2}{L}\operatorname{sech}^2\left[\frac{-g\bar{k}}{T_0}\left\{t - \frac{T_0}{gL_0}z(1-2\bar{k}^2) + \frac{\lambda\varepsilon^{5/2}z^2}{8gL_0^2}\right\} + \theta\right] \tag{47}$$

and

$$u(z,t) = R_0\bar{u}_0 + \frac{6R_0\bar{k}^2}{M}\operatorname{sech}^2\left[\frac{g\bar{k}}{T_0}\left\{t - \frac{T_0}{gL_0}z(1-2\bar{k}^2) + \frac{\lambda\varepsilon^{5/2}z^2}{8gL_0^2}\right\} + \theta\right]. \tag{48}$$

Further, making use of (48), from (5) we obtain

$$R(z,t) = R_0 - \tan\alpha z + R_0\bar{u}_0 + \frac{6R_0\bar{k}^2}{M}\operatorname{sech}^2\left[\frac{g\bar{k}}{T_0}\left\{t - \frac{T_0}{gL_0}z(1-2\bar{k}^2) + \frac{\lambda\varepsilon^{5/2}z^2}{8gL_0^2}\right\} + \theta\right]. \tag{49}$$

The soliton solution represents a pulsatile disturbance given by a relation between the amplitude and the pulse wave velocity. The stroke volume Q of the blood pulse is given by

$$Q = \int_0^T Av\,\mathrm{d}t \tag{50}$$

where T denotes the period of the pulse; its value is 0.6 s for thoracic aorta of living dogs [30].

5. Numerical results and observations

With a view to examining the validity of the analytical solution presented above, let us consider a specific numerical example in order to perform some relevant computational work. The experimental data available in the literatures (cf. [30,32–37]) for the middle descending thoracic aorta of living dogs are as follows:
$\rho = 1.05$ g/cm^3, $\rho_0 = 1.06$ g/cm^3, $a = 1.95$, $v_m = \frac{1}{2}v^* = 55$ cm/s,
$p_m - p_A = 102$ mmHg, $p_0 - p_A = 81$ mmHg, $R_0 = 0.55$ cm,

$$u_m/R_0 = 0.2, \qquad h_0/R_0 = 0.12, \qquad E = 5.49 \times 10^6 \text{ dynes/cm}^2. \tag{51}$$

The suffix 'm' indicates the corresponding maximum value. Using these data the parameters L_0, T_0, p_0 and C_0 defined in (11) are estimated by using (51) as

$$L_0 = 0.1354 \text{ cm}, \qquad T_0 = 2.417 \times 10^{-4} \text{ s}, \qquad C_0 = 1120 \text{ cm/s} \quad \text{and}$$
$$p_0 = 658\,800 \text{ dynes/cm}^2 = 494 \text{ mmHg}. \tag{52}$$

The value $\bar{p}_0$ which corresponds to the lowest blood pressure $p_0 - P_A = 81$ mmHg is estimated by (15) with the help of (52) as

$$\bar{p}_0 = 0.164. \tag{53}$$

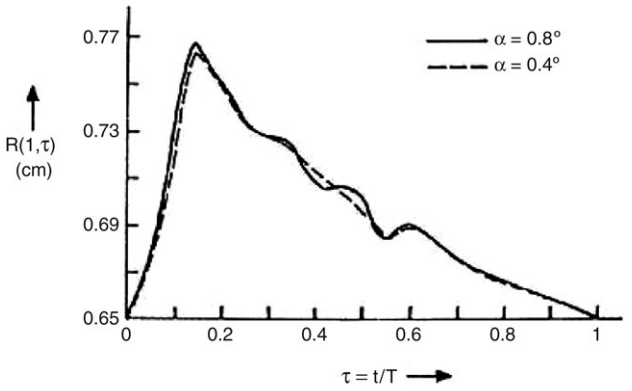

Fig. 3. Variation of $R(\tau)$ with the non-dimensional cardiac period τ.

The corresponding value of $\bar{u}_0$ is calculated by using (18) and (53) as

$$\bar{u}_0 = 0.1685. \tag{54}$$

The estimated the values of the parameters g, K, L, M and N obtained from (19) and (42) are

$$g = 1.044, \qquad K = 2.048, \qquad L = 1.96, \qquad M = 1.83, \qquad N = 1.2424. \tag{55}$$

From the solitary wave solutions given by (46)–(48), we obtain

$$v_m = 6C_0\bar{k}^2/K, \qquad p_m = p_0 + 6p_0\bar{k}^2/L, \qquad u_m = R_0\bar{u}_0 + 6R_0\bar{k}^2/M. \tag{56}$$

Employing the relevant experimental data given in (51) and using (52), (53) and (55) we estimate $\bar{k} = 0.1295, 0.118, 0.098$ from the three relations given by (56). The arithmetic mean of the three above-written values is taken as the value of the parameter $\bar{k}$. Thus for the present computational work, we take $\bar{k} = 0.115$. Using the values of L_0 and R_0 we estimated by using (26) the values of the small parameter ε for different semi-angles of taper $\alpha = 0.4°$ and $\alpha = 0.8°$ as follows:

$$\varepsilon = \begin{cases} 0.078 & \text{for } \alpha = 0.4° \\ 0.1034 & \text{for } \alpha = 0.8°. \end{cases}$$

The significance of the precise values of α should not be taken too seriously; its experimental determination is difficult and is liable to appreciable errors [1]. Also, in reality α is a function of z and t; our assumption of a constant value of α is, therefore, not above board; however, due to lack of adequate experimental data, there is hardly any alternative better than this.

Fig. 3 gives the numerical values of the radius of the aorta at different instants of a cardiac cycle for different taper angles of the aorta, when a wave propagates through it. These results indicate that the minimum value of the radius is 0.65 cm (for $\alpha = 0.8°$) at the beginning of the cycle and that there is a sharp increment in the radius of the blood vessel in the time interval $0 \le \tau \le 0.144$. It attains the maximum value 0.766 cm at $\tau = 0.144$, then decreases gradually until $\tau = 0.55$. In the interval of time $0.55 \le \tau \le 0.6$, the radius increases slightly and attains a local maximum there; then it decreases monotonically and attains its minimum at $\tau = 1$. We further notice that the effect of the taper angle on the radius of the blood vessel is negligibly small near the end of a cardiac cycle at least within the purview of the present study. In Figs. 3–6, the solid lines represent the variation when the semi-taper angle $\alpha = 0.8°$, while the broken lines give the same when $\alpha = 0.4°$.

So far as the variations of the rate of change of radius of the aorta within a cardiac period is concerned, it is observed (cf. Fig. 4) that the rate of change of radius increases sharply from 0 to its maximum value 18 (for $\alpha = 0.8°$) in the interval of time $0 \le \tau \le 0.135$ and then decreases sharply to a locally minimum value -2 within a time interval $0.135 \le \tau \le 0.25$. Gradually it increases further until $\tau = 0.29$ and then decreases to attain the minimum value -7 at $\tau = 0.4$. In the interval of time $0.4 < \tau < 0.47$, it again increases sharply and then its value oscillates with smaller amplitudes upto $\tau = 1$. Furthermore, it is also observed from the figures that the taper angle of the aorta bears the potential to considerable affect the rate of change of radius only in the interval of time $0.05 < \tau < 0.6$.

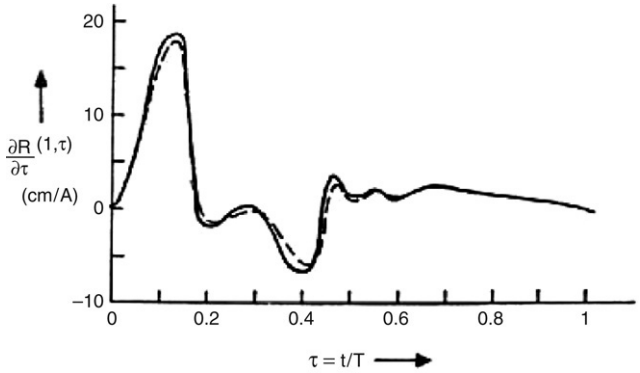

Fig. 4. Variation of the rate of change of radius with the non-dimensional cardiac period τ.

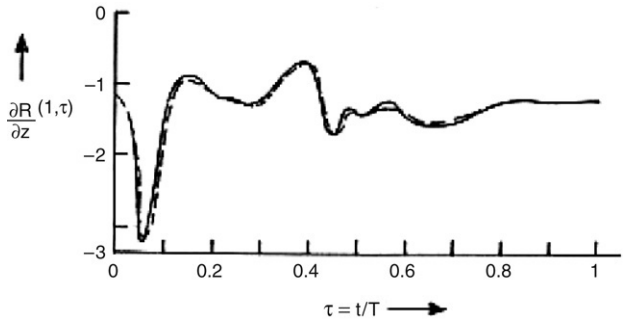

Fig. 5. Variation of the longitudinal change of radius with the non-dimensional cardiac period τ.

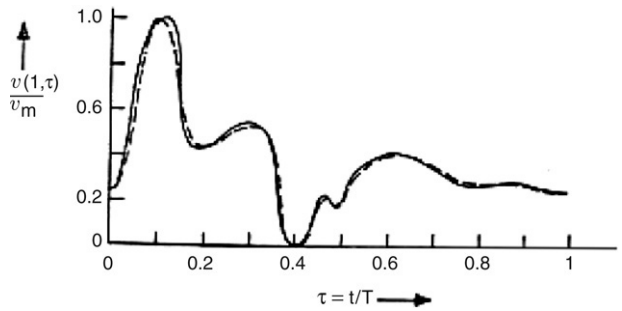

Fig. 6. Variation of the non-dimensional axial velocity with the non-dimensional cardiac period τ.

Fig. 5 gives the rate of change of radius of the aortic segment with respect to the longitudinal coordinate at different instants of a cardiac cycle. It may be observed that throughout a cardiac cycle, it is negative (both for $\alpha = 0.4°$ and $0.8°$); at the beginning of a cardiac cycle its value is equal to -1.2. As time progresses, its value decreases sharply to the value -3.2 (for $\alpha = 0.8°$) at $\tau = 0.055$ and then increases sharply to the value -0.87 at $\tau = 0.15$. It then shows a decreasing trend for some time and then increases continuously upto $\tau = 0.39$ to attain its maximum value -0.66. In the time interval $0.39 < \tau < 0.45$ its value again decreases sharply and then oscillates with small amplitudes upto the end of the cycle. Its value at the end of the cardiac cycle is the same as that at the beginning, viz. -1.2. In this case also the angle of taper has little influence on the longitudinal change of radius, particularly towards the end of a cardiac cycle.

Fig. 6 depicts the nature of variation of the axial velocity at a fixed location ($z = 1$) of the aortic segment under consideration within a cardiac cycle. It reveals that at the beginning (as well as at the end) of the cycle the non-dimensional axial velocity is equal to 0.235; subsequently it increases sharply and attains its maximum value 1 at $\tau = 0.1$ (for $\alpha = 0.8°$). Then it decreases sharply upto $\tau = 0.2$ and then for sometime it increases gradually, then decreases sharply to its minimum value 0, at $\tau = 0.41$. After this it increases gradually upto $\tau = 0.62$ and

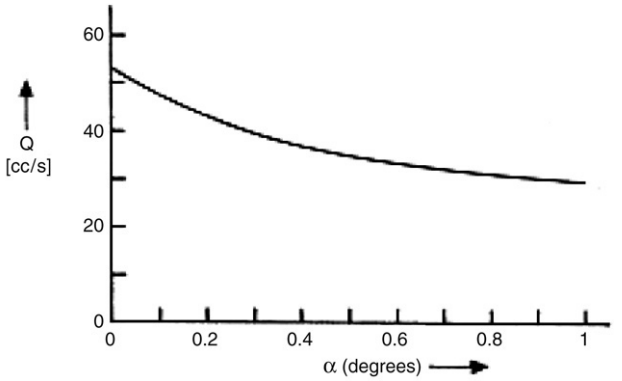

Fig. 7. Variation of the stroke volume Q vs. taper angles.

Table 1
Comparison of the non-dimensional axial velocity (ratio between the axial velocity and its maximum) in the present theoretical study with the experimental results of Ling et al. [17] for different taper angles and for different cardiac outputs

Non-dimensional cardiac period	Results of the present theoretical study		Results of the experimental study of Ling et al. [17]	
τ	$\alpha = 0.4°$ Cardiac output 2.2 l/min	$\alpha = 0.8°$ Cardiac output 1.8 l/min	$\alpha = 0.4°$ Cardiac output 5.7 l/min	$\alpha = 0.8°$ Cardiac output 2.6 l/min
0.0	0.25	0.25	0.19	0.05
0.1	1.00	1.00	1.00	1.00
0.2	0.44	0.43	0.68	0.60
0.3	0.53	0.55	0.40	0.50
0.4	0.00	0.00	0.30	0.06
0.5	0.21	0.22	0.25	0.15
0.6	0.40	0.42	0.20	0.23
0.7	0.36	0.35	0.18	0.01
0.8	0.29	0.28	0.18	0.00
0.9	0.28	0.29	0.19	0.06
1.0	0.25	0.25	0.19	0.05

then continuously decreases to the value 0.235 at $\tau = 1$. Here we find that the taper angle alters the axial velocity throughout a cardiac cycle.

Fig. 7 shows the dependence of the volume flow per cycle (Q) on the taper angle, for $0° \leq \alpha \leq 1°$ at $z = 1$. This figure illustrates that the stroke volume is maximum if the aorta be of uniform radius and that the volume flow decreases continuously as the semi-taper angle α increases gradually upto 1°.

6. Discussion

Fig. 1 gives a comparison of our results computed on the basis of the theoretical model developed and analysed in this paper using available experimental data available in existing scientific literatures with those of experimental finding reported by Ling et al. [17]. It reveals from this table that in the present theoretical study, for semi-angle of taper 0.4° with the cardiac output of 2.2 l/min the graph of the axial velocity has an increasing tendency in the time interval $0 < \tau < 0.1$, decreasing in $0.1 < \tau < 0.2$, increasing in $0.2 < \tau < 0.3$, decreasing in $0.3 < \tau < 0.4$, increasing in $0.4 < \tau < 0.6$ and again decreasing in $0.6 < \tau < 1$, whereas for the same angle of taper with the cardiac output of 5.7 l/min the experimental study of Ling et al. [17] shows that the graph of the axial velocity is increasing in $0 < \tau < 0.1$, decreasing in $0.1 < \tau < 0.8$ and increasing in $0.8 < \tau < 1$. This difference in the nature of variation of axial velocity is presumably owing to the considerable difference in consideration of cardiac output.

Table 1 further shows that for the semi-angle of taper 0.8° our theoretical predictions for the nature of variation in axial velocity for a cardiac output of 1.8 l/min are in fair agreement with the experimental results of Ling et al. [17]

for the cardiac output of 2.6 l/min (except for $\tau = 0.3$). when the difference between the cardiac outputs is smaller. Thus it may be calculated that our theoretical model is more particularly valid in the small range of cardiac input.

Acknowledgement

One of the authors (J. C. Misra) is grateful to the Council of Scientific and Industrial Research, New Delhi for the financial support.

References

[1] S.C. Ling, H.B. Atabek, J. Fluid Mech. 55 (1972) 493–511.
[2] J.K.-J. Li, J. Melbin, R.A. Riffle, A. Noordergraaf, Circ. Res. 49 (1981) 442–452.
[3] C.J.H. Jones, K.H. Parker, R. Hughes, D.J. Sheridan, J. Biomech. Engrg. 114 (1992) 10–14.
[4] R.H. Cox, J. Biomech. 2 (1969) 251–265.
[5] S. Noubissie, P. Woafo, Phys. Scripta 69 (2004) 249–256.
[6] H. Demiray, H. Dost, Int. J. Phys. Engrg. Sci. 50 (1998) 201–210.
[7] H. Demiray, Z. Angew. Math. Phys. 49 (1998) 538–557.
[8] Y. Hashizume, J. Phys. Soc. Japan 57 (1988) 4160.
[9] S. Yomosa, J. Phys. Soc. Japan 56 (1987) 506.
[10] J.C. Misra, S.K. Pandey, Comput. Math. Appl. 43 (2002) 1183–1193.
[11] D.L. Fry, D.M. Griggs, J.C. Greenfield, E.O. Attinger (Eds.), Pulsatile Blood Flow, McGraw-Hill, 1964, p. 101.
[12] S.C. Ling, H.B. Atabek, J.J. Carmody, in: M. Hetenyl (Ed.), Pulsatile Flows in Arteries, Springer, New York, 1969, p. 227.
[13] J.C. Misra, S. Chakravarty, J. Biomech. 19 (1986) 907–918.
[14] J.C. Misra, B.K. Sahu, Math. Comput. Modelling 12 (1989) 333–349.
[15] J.C. Misra, M.K. Patra, J. Biomech. 26 (1992) 1129–1141.
[16] S.C. Ling, AIAA 70 (1970) 789.
[17] S.C. Ling, H.B. Atabek, W.G. Letzing, D.J. Patel, Circ. Res. 33 (1973) 198–212.
[18] D.J. Patel, J.C. Greenfield, D.L. Fry, In vivo pressure length radius relationship in certain blood vessels in man and dog, in: E.O. Attinger (Ed.), Pulsatile Blood Flow, McGraw-Hill, New York, 1964, p. 277.
[19] D.J. Patel, D.L. Fry, Circ. Res. 19 (1966) 1011–1021.
[20] H.B. Atabeck, Biophys. J. 8 (1968) 626–649.
[21] H. Wolinsky, S. Glowov, Circ. Res. 14 (1964) 400–413.
[22] C.S. Gardner, G.K. Morikawa, Similarity in the asymptotic behaviour of collision-free hydromagnetic waves and water waves, Courant Inst. Math. Sci. Rep. NYO - 9082, 1960, pp. 1–30.
[23] T. Taniuti, H. Washini, Phys. Rev. Lett. 21 (1968) 209–212.
[24] T. Taniuti, N. Yajima, J. Math. Phys. 10 (1969) 1369–1372.
[25] T. Taniuti, C.C. Wei, J. Phys. Soc. Japan 24 (1968) 941–946.
[26] C.S. Gardner, J.M. Greene, M.D. Kruskal, R.M. Miura, Phys. Rev. Lett. 19 (1967) 1095–1097.
[27] P.D. Lax, Comm. Pure Appl. Math. 21 (1968) 467–490.
[28] M. Wadati, M. Toda, J. Phys. Soc. Japan 32 (1972) 1403–1411.
[29] M. Wadati, J. Phys. Soc. Japan 32 (1972) 1681.
[30] D.A. Mc Donald, and E. Arnold (Eds.), Blood Flow in Arteries, 2nd edn., London, 1960, p. 1974.
[31] K. Nozaki, T. Taniuti, J. Phys. Soc. Japan 34 (1973) 796–800.
[32] D.J. Patel, F. Defreties, J.C. Greenfield Jr., D.L. Fry, J. Appl. Physiol. 18 (1963) 1111–1117.
[33] D.H. Bergel, The viscoelastic properties of the arterial wall, Ph.D. Thesis, University of London, 1960.
[34] B.S. Gow, R.E. Taylor, Circ. Res. 23 (1968) 111–122.
[35] L.H. Peterson, R.E. Jenson, J. Rarnell, Circ. Res. 8 (1960) 622–639.
[36] D.H. Bergel, J. Physiol. 156 (1961) 445–457.
[37] D.H. Bergel, J. Physiol. 156 (1961) 458–469.